Indian Journal of Marine Sciences
Vol. 39(1), March 2010, pp. 15-26

Assessment of surface circulation using remote-sensed data, in-situ measurements and directional statistics

G Kalantzi[1]*, T H Soukissian[2], K Nittis[2]

*[1]Ocean Observing and Climate group, National Oceanography Centre, Southampton, European Way, Southampton, SO14 3ZH,
[2]United Kingdom Hellenic Centre for Marine Research, Institute of Oceanography, PO BOX 712, Anavyssos Greece
[E-mail: *gxk@noc.soton.ac.uk, tsouki@ath.hcmr.gr]

Received 21 April 2008; revised 7 April 2009

A method accounting for the directional characteristics of in-situ wind and current measurements is proposed and applied in two characteristic locations of the Aegean Sea. With the combined use of directional statistics, satellite derived SST maps and in-situ measurements, an efficient quantitative description of the directional current behavior and its relation with the corresponding wind fields, thermohaline trends, seasonality and sources of the main meso- and large-scaled surface currents of the Aegean Sea, is elaborated. The evolution, persistence, duration and signal of the surface circulation patterns has been appeared to be quite different during each season or calendar year, shaping in this way a completely different layout of the overall sea surface circulation. This is a novel approach interrelating directional statistics with in-situ measurements and SST maps, for the Aegean Sea.

[**Keywords:** surface circulation, satellite SST data, directional statistics, Aegean Sea, POSEIDON system]

Introduction

Remote-sensed data is being routinely used to monitor the marine environment over a wide range of time/space scales and parameters[1]. Its value increases when it is combined with in-situ data for calibration, validation and/or assimilation purposes and for extrapolation of the surface information to deeper layers. In this paper an example of such a combined use of satellite radiometer Sea Surface Temperature (SST), in-situ upper layer measurements and directional statistics analysis is presented. The aim of the work are

i) the description of the general surface circulation of the Aegean Sea using in-situ and remote sensed data for a period of 2 years, 01/06/2000-31/05/2002 in combination with
ii) the directional statistics analysis of in-situ current data for two locations in the North and South Aegean Sea, for the same time period.

The general circulation of the Aegean Sea (Fig. 1), as well as of the whole Eastern Mediterranean region is characterized by multiple scaled patterns that include: (i) a basin scale cyclonic flow, defining the overall thermohaline cell, (ii) a sub-basin scale, defining the gyres of the main thermocline connected by intense jets and meandering currents, and (iii) the very energetic mesoscale eddy field modulating the two previous scales through complex non-linear interactions[2]. Aegean Sea is a highly-dynamical and active area with unique physiographic and hydrodynamic characteristics, which also affects the general circulation of the Eastern Mediterranean Sea as an important source of intermediate and deep water masses[3-6].

South Aegean Sea exchanges waters with the Eastern Mediterranean through the straits of the Cretan Arc: the Rhodes, Karpathos and Kassos Straits to the east and the Kithyra and Antikithyra Straits to the west. The dominant surface pattern is the inflow of the saline and warm Levantine Surface Water (LSW) that enters through the eastern straits and moves cyclonically towards north, along the Asia Minor coasts. North Aegean Sea receives the low salinity and nutrient rich Black Sea Water (BSW) that enters the basin through the Straits of Dardanelles and influences the general surface circulation and hydrology of the area. North Aegean is also influenced by seasonal major river outflows discharging fresh water in the sea[2,7-11].

The Kiklades Plateau in the central part of the Aegean Sea is dominated by reverse flow phenomena;

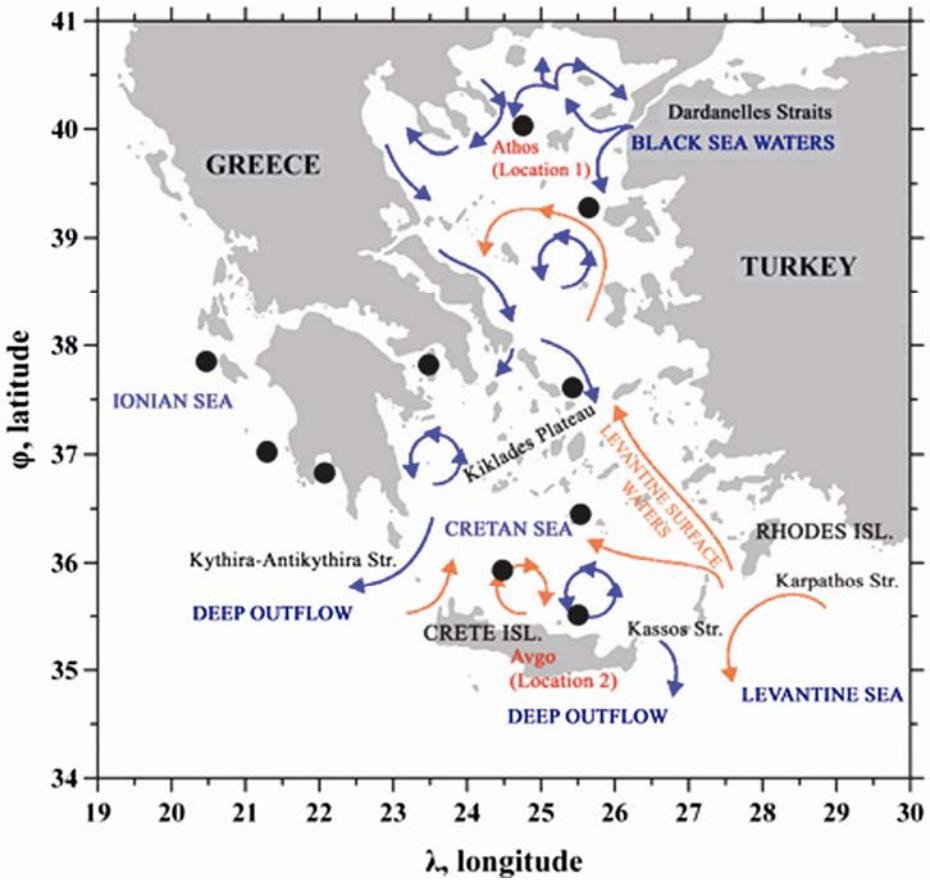

Fig. 1—General circulation patterns of the Aegean Sea and the POSEIDON network (the buoy locations are represented as circles)

thus it can be characterised as an intermediate area where different types of water masses (with specific temperature and salinity characteristics) originating from the northern and the southern regions, interact. Due to the specific geomorphology, this Plateau becomes the main natural barrier of the Aegean Sea and a very energetic location due to the above mentioned interactions. The basic circulation characteristics of the area have been firstly revealed through a series of research cruises conducting synoptic CTD sampling during the 80s and 90s.

The present study had been presented in a specific pattern and consists (1) the data and associated methods (2) the temporal evolution of the circulation characteristics through combined analysis of SST images and in-situ wind, current and temperature measurements (3) the directional statistical analysis of surface currents in two characteristic locations of the Aegean Sea

Materials and methods

In-situ measurements

The in-situ measured data used in this work was obtained from the POSEIDON buoy network. POSEIDON is a real-time monitoring and forecasting system for the marine environmental conditions in the Aegean Sea[12]. The observation network consists of 11 oceanographic buoys measuring meteorological and oceanographic parameters. The data analyzed herein corresponds to two characteristic locations (Fig. 1):

(i) Sou th-east of Athos Peninsula (39.96°N, 24.72°E; this location will be mentioned hereafter for brevity as **Location 1**),

(ii) North of Crete Island (35.37°N, 25.38°E, Avgo Islet; **Location 2**).

Location 1 has been selected because it is situated in a highly active area due to the dominance of two major thermohaline movements during stratification seasons: i) the inflow of the cool Black Sea Water (BSW) and ii) the north-east coastal movements of warm waters remaining in the area from previous seasons. On the other hand, location 2 has been selected because it is situated in an area where, during the same seasons, a very energetic surface dipole system prevails (north of Crete Island).

To efficiently deal with the surface circulation study of the Aegean Sea and the directional statistical

analysis of in-situ current measurements, four different environmental parameters in the form of time series, are considered. The parameters are ,

1 water temperature measured in-situ at six different water depths (3, 10, 20, 30, 40, 45m);
2 air temperature measured at 3m height above the sea surface;
3 wind speed and direction measured at 3m height above the sea surface, and
4 current speed and direction measured at 3m depth.

All the corresponding time series are of the same length, namely two years: 01/06/2000-31/05/2002.

The data were pre-processed to identify possible errors using the following criteria:

a) The occurrence of the sensors default value in the field of the record; this value indicates that the measurement procedure was not properly activated or implemented.
b) Values remaining exactly the same for more than three consecutive records, i.e. within a time period of 9 hours. This problem usually results from stucks in the sensor's buffer.

Remote-sensed data

The remote-sensed data comprises of 24 appropriately processed SST images, each one corresponding to one monthly composite. The images correspond to the entire Aegean Sea region for the examined time period of two years.

The primary data was recorded from the AVHRR radiometer embodied on NOAA 14 satellite. The partly processed data was downloaded from the on-line data base of the German Aerospace Centre (DLR), http://isis.dlr.de. The major processing steps before the data can be accessed by users, provided by the DLR-EOWEB metadata system, are (Fig. 2):

1 **Automatic pre-navigation and interactive supervision.** A process of autonavigation is performed using WDB-II coastline and river data to improve the accuracy of the geo-referenzation.
2 **Calibration.** The solar channels (used for cloud detection) are calibrated into % technical albedo as described by NOAA, while the thermal infrared data (channels 3, 4 and 5) is converted from raw counts to radiances with a linear relationship based on the raw count values associated with cold space and an onboard blackbody. The infrared radiances are converted to brightness temperatures (Celcius deg.) using the inverse Planck function.
3 **Cloud Screening and clearing.** To ensure that SST values are derived only for cloud-free water surfaces a couple of cloud tests are performed based on the principal characteristics of water bodies and considering typical spectral and textural parameters (e.g. dark, warm and homogeneous surface).
4 **Derivation of the Multi-channel Sea Surface Temperature (MSST).** The applied formula is based on the brightness temperatures of AVHRR channels 4 and 5[13]. This technique is known as the "Split Window Technique" and corrects atmospheric attenuation caused by absorption of water vapour (this phenomenon leads to a significant drop, up to 8ºC, in derived brightness temperatures).
5 **Remapping.** The data is remapped into standard Mercator projections with a given geometrical resolution of 1.1132 km at the centre of the satellite map (for the Mediterranean: 39.0°N-16.5°E).

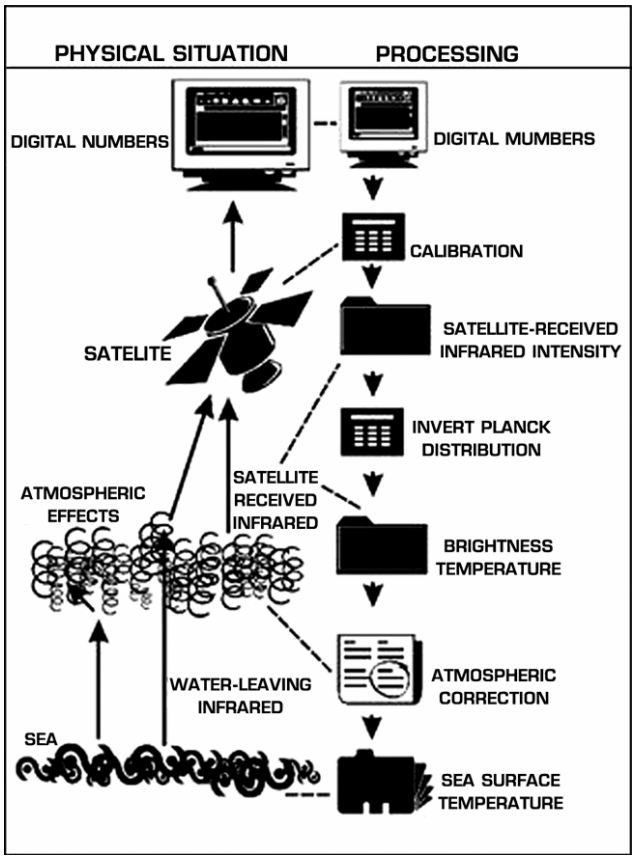

Fig. 2—AVHRR data processing

6 **Composing and Synthesis.** Three daily maps are composed using up to seven different NOAA acquisitions. They are composed together according to the maximum temperature value given at every pixel's position to minimize cloud coverage. Weekly and monthly maps are derived from the daily maximum images using the average at every pixel's position.

7 **Ocean masking.** A WDB-II based land/sea mask in 1 km geometrical resolution is used to mask out remaining SST values over land areas.

8 **Integer and scaling.** The SST data is scaled from its original 10-bit format into a user-friendly 8-bit integer format (values from 0 to 255). The SST values are stored as follows: grey-value "0" is referred to "Land" and grey-value "255" is reserved for "Cloud" or "No Data". The temperature range starts with "0.125" Celcius deg. and is referred to grey-value "1". The radiometric resolution is "0.125" Celcius deg. and therefore grey-value "254" is referred to "31.75" Celcius deg. (maximum temperature).

After downloading the partly processed data (24 8-bit _.tiff files of the Aegean Sea representing mean monthly composites), 24 coloured maps exhibiting clearly the sea surface temperature chart had to be created. Firstly, the _.tiff files were transformed into grid files and afterwards the predefined temperature scale (8^{th} step of the processing) was applied to the grid files so that every pixel of the file to correspond to a certain temperature value. Finally, specific temperature ranges were assigned to specific colours and the sea surface patterns, such as cyclones, anticyclones, general surface movements, interactions, inflows, outflows etc, were appropriately highlighted.

In the next section some elements of the directional statistics theory will be provided. Directional statistics will be applied for the analysis of in-situ measured surface current and wind parameters.

Simple statistical parameters of circular data

Clearly, the statistics used for analyzing linear data is not directly applicable to circular data. Directional statistics is a special topic of the statistical theory which deals with circular data[14-17]. In this section we will present the main parameters of directional data samples and the most important correlation coefficients between circular-circular and linear-circular random variables.

Mean direction, concentration and dispersion

Let $\theta_i,\ i=1,2,...,n$ be the directions of some given unit vectors. The mean direction $\bar{\theta}$ (i.e., the direction of the resultant vector), the circular variance $V(\theta)$ and the circular standard deviation $SD(\theta)$, of $\theta_i,\ i=1,2,...,n$ are given as follows:

$$\bar{\theta}=\begin{cases}\tan^{-1}\left(\frac{1}{n}\sum_{i=1}^{n}\sin(\theta_i)\Big/\frac{1}{n}\sum_{i=1}^{n}\cos(\theta_i)\right), \\ \qquad\qquad \text{if } \frac{1}{n}\sum_{i=1}^{n}\cos(\theta_i)\geq 0 \\ \tan^{-1}\left(\frac{1}{n}\sum_{i=1}^{n}\sin(\theta_i)\Big/\frac{1}{n}\sum_{i=1}^{n}\cos(\theta_i)\right)+\pi, \\ \qquad\qquad \text{if } \frac{1}{n}\sum_{i=1}^{n}\cos(\theta_i)<0,\end{cases} \quad \ldots (1)$$

provided that

$$\bar{R}=\sqrt{\left(\frac{1}{n}\sum_{i=1}^{n}\cos(\theta_i)\right)^2+\left(\frac{1}{n}\sum_{i=1}^{n}\sin(\theta_i)\right)^2}>0, \quad \ldots (2)$$

$$V(\theta)=1-\bar{R}, \quad \ldots (3)$$

and

$$SD(\theta)=\sqrt{-2\log\bar{R}}. \quad \ldots (4)$$

For values of $\bar{R}$ close to 1, the directions $\theta_i,\ i=1,2,...,n$ are tightly clustered, while for values close to 0 the directions are widely dispersed.

The concentration parameter $\hat{k}$ is a measure of the spreading of the von Mises angular distribution (the analogous of the Gaussian distribution for linear data) and can be approximately estimated as follows:

$$\hat{k}=\begin{cases}2\bar{R}+\bar{R}^3+5\bar{R}^5/6, \ if\ \bar{R}<0.53 \\ -0.4+1.39\bar{R}+0.43/(1-\bar{R}), \ if\ 0.53\leq\bar{R}<0.85 \\ 1/(\bar{R}^3-4\bar{R}^2+3\bar{R}), \ if\ \bar{R}\geq 0.85.\end{cases} \quad \ldots (5)$$

A high value of $\hat{k}$ indicates a tightly coupled distribution and a low value corresponds to a wide-spreaded distribution.

Measures of correlation

The association between a linear and a circular random variable can be measured by means of the *linear-circular correlation coefficient*, while the association between two circular variables by the *circular-circular correlation coefficient*. The sample version of the circular-circular correlation coefficient for two directional random variables θ and φ is defined as follows[15]:

$$r_T = \frac{\sum_{1\le i\le j\le n} \sin\left(\theta_i - \theta_j\right)\sin\left(\varphi_i - \varphi_j\right)}{\sqrt{\sum_{1\le i\le j\le n} \sin^2\left(\theta_i - \theta_j\right) \sum_{1\le i\le j\le n} \sin^2\left(\varphi_i - \varphi_j\right)}}, \quad \ldots (6)$$

where $\theta_i,\ i=1,2,...,n$ and $\varphi_j,\ j=1,2,...,n$, are realizations of θ and φ respectively. A large value of $|r_T|$ suggests the rejection of the independence assumption between θ and φ.

The linear-circular association refers to the linear dependence of $E\left[X|\theta\right]$ on θ, where $E[\cdot]$ denotes the mean value operator, X is a scalar random variable and θ is a circular one with realizations x_i and θ_i, $i=1,2,...,n$, respectively. Then, the linear-circular correlation coefficient R_n^2 is defined as follows:

$$R_n^2 = \frac{\left(r_{12}^2 + r_{13}^2 - 2r_{12}r_{13}r_{23}\right)}{1-r_{23}^2}, \quad \ldots (7)$$

where

$$r_{12} = r\left[(x_1,\cos\theta_1),\ldots,(x_n,\cos\theta_n)\right],$$
$$r_{13} = r\left[(x_1,\sin\theta_1),\ldots,(x_n,\sin\theta_n)\right],$$
$$r_{23} = r\left[(\cos\theta_1,\sin\theta_1),\ldots,(\cos\theta_n,\sin\theta_n)\right]$$

and

$$r\left[(u_1,v_1),\ldots,(u_n,v_n)\right] = \frac{\sum_{i=1}^{n}(u_i-\bar{u})(v_i-\bar{v})}{\sqrt{\sum_{i=1}^{n}(u_i-\bar{u})^2 \sum_{i=1}^{n}(v_i-\bar{v})^2}},$$

where $\bar{u} = \sum_{i=1}^{n} u_i/n, \quad \bar{v} = \sum_{i=1}^{n} v_i/n$

Results

Assessment of in-situ temperature time series

In Fig. 3 and Fig. 4 the evolution of water temperature (at depths 3, 10, 20, 30, 40, 45m) and wind speed, for locations 1 and 2 during the two-year period (June 2000-May 2002) are presented. It should be mentioned that the data gaps in the diagrams are due either to the filtering process of the time series, or to missing values due to buoy maintenance periods.

The seasonal variability is the dominant characteristic of both locations. During May and until the first days of June the ongoing heating of the seawater leads to an extensive stratification which settles in a rather short time, throughout the upper layers of the sea. This stratification results from the onset of the seasonal thermocline which dominates the upper layers until its breakdown approximately at the beginning of November. The strongest stratification can be detected from the beginning of July until mid-October indicating very high stability. More precisely, during stratification periods each layer maintains a certain temperature status and only few limited incidents associated with mechanical mixing during strong wind conditions are present (see e.g. August 2001 at location 1).

Gradual change from heating to cooling during autumn and the increasing wind potential leads to the thermocline destruction at early November. Strong stratification is followed by strong mixing and homogeneous temperature conditions throughout the upper layers until the heating process starts again, approximately at mid-May. During the mixing months the temperature variations are minimal compared to those during the thermocline ones (during the mixing periods at location 1 temperature varies only from 12ºC to 15ºC, while at location 2 only from 15ºC to 17ºC).

For simplicity reasons, the time period from June 2000 to November 2000 will be referred hereafter as Season B2000, from December 2000 to May 2001 as Season A2001, from June 2001 to November 2001 as Season B2001 and from December 2001 to May 2002 as Season A2002. It is clear that these seasons coincide with the periods of stratification (B seasons) and mixing (A seasons) conditions.

During B seasons the temperature field in the thermocline layer reveals high-frequency oscillations at a time scale of the order of 10 to 20 days. These oscillations are most probably associated with the presence of downwelling/upwelling phenomena and

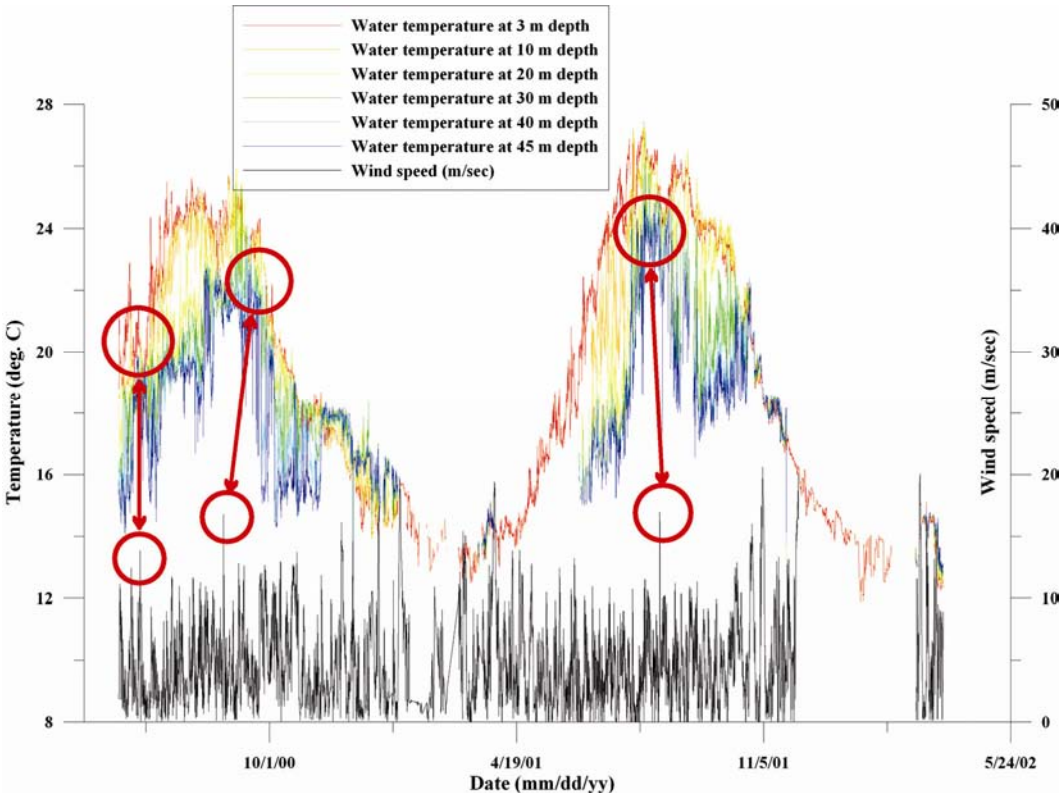

Fig. 3—Time-temperature-wind diagram for location 1

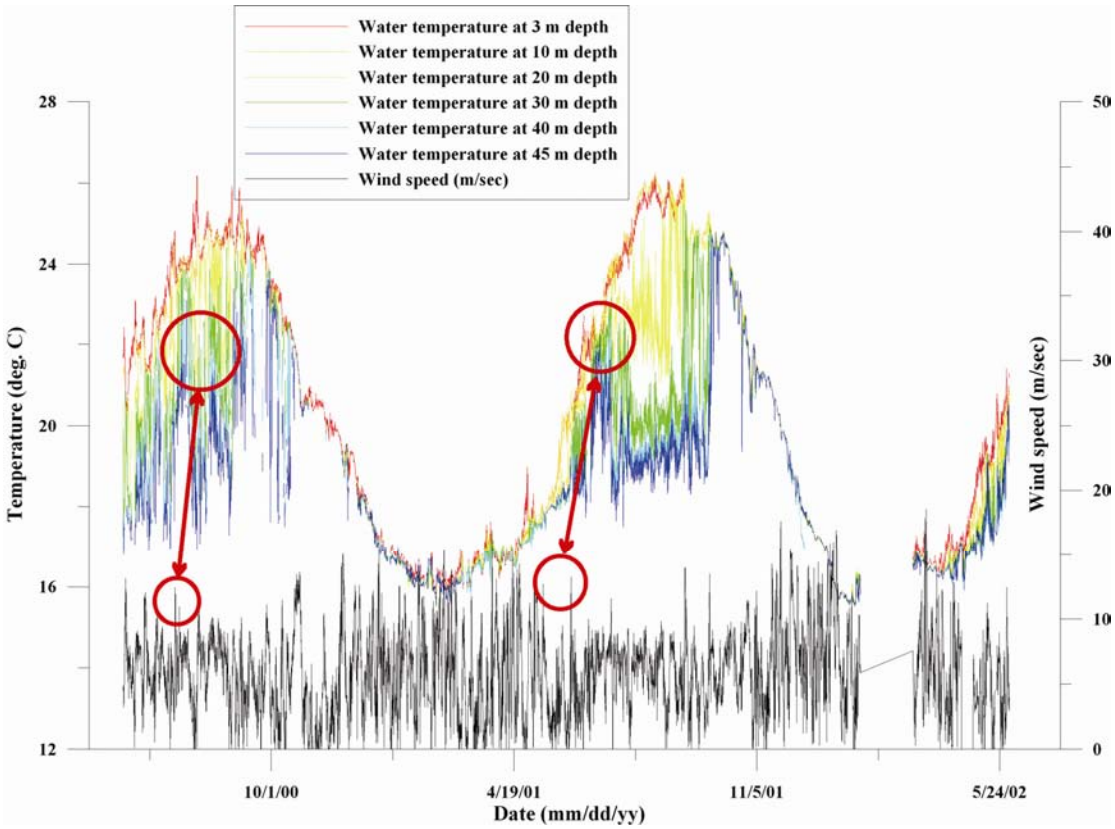

Fig. 4—Time-temperature-wind diagram for location 2

cyclonic/anticyclonic wind driven eddies. These interactions at locations 1 and 2 are also evident on the SST maps presented in the next subsection.

Many of the temperature abrupt changes observed within the upper layers are induced from changes in local wind fields. For example, strong winds can cause intense mixing vertically with depth or horizontally breadthways large surface areas. Fig. 3 and Fig. 4 reveal that some unexpected temperature oscillations and mixing incidents during the stratification seasons occur in correspondence with strong wind fields. During August 2000 and August 2001 at location 1 periods of homogeneous temperature within the thermocline stratification are evident. These incidents are most likely associated with the strong winds blowing during the same time period. Some of these incidents are encircled in Fig. 3 for location 1 and Fig. 4 for location 2.

It was found that the water temperature flux of the surface layer is fairly dependent on the air temperature trend. Though, due to the higher heat capacity of the water, the water temperature evolution is much smoother than the corresponding air temperature. Moreover, during the A seasons and probably due to the strong mixing effect, the intense fluctuations of the air temperature seem to affect in a minor degree, the more equable water temperature behaviour.

SST maps, currents and wind conditions in locations 1 and 2

The maps presented (in Fig. 5 and Fig. 6) refer to the spatial distribution of SST for two typical months for each of the four seasons B2000, A2001 (in Fig. 5), B2001 and A2002 (in Fig. 6). These maps are used to examine the structure and variability of the surface circulation in the time and space domains.

During A seasons the mixing conditions that dominate the water column, affect also the sea surface circulation patterns and thus weaken the signal of large and meso-scale surface eddies and bifurcations. The main structures that can be detected are: a) the Rhodes cyclone to the SE of Rhodes Island, b) the Pelops anticyclone to the SW of Peloponnesus and c) part of the Ierapetra anticyclone. The large scale temperature pattern divides the Aegean Sea into two discrete regions: i) the cool north-west region and ii) the warmer central and south-east region. This contrast is the result of: a) the north-south heat flux gradient, b) the influence by the cold BSW that enters through the Dardanelles Straits and moves cyclonically southwards along the north and west Aegean coasts and c) the influence of the warm and saline LSW transported by the Asia Minor current that enters through the Rhodes and Karpathos Straits and moves northwards along the eastern Aegean coasts. A branch of this current occasionally moves westwards after its entrance, affecting the temperature field of the eastern Cretan Sea (Fig. 5, March 2001).

On the other hand, during B seasons the strong stratification intensifies the mesoscale structures that dominate the surface circulation of South Aegean Sea. The Rhodes cyclone is much better defined and the same holds also for the Cretan Sea dipole system where both the cyclonic and anti-cyclonic gyres are now visible. This is not the case for the Pelops Gyre, which occasionally moves westwards (outside the domain covered by the SST maps) or has a very weak surface signal during summer[18]. During the same period the parts of two strong gyres are detected south of Crete: the Cretan cyclone to the west and the very energetic Ierapetra anticyclone to the east.

The large scale temperature contrast of A season (warm SE - cold NW) is replaced during B season by two different patterns: a) the strong east-west contrast generated by the intense upwelling of the eastern Aegean Sea during the months of strong Etesian winds (July to September) and b) a north-south gradient similar to the one of A season generated during the transitional period between the two seasons. The effect of the BSW and LSW inflow into the Aegean is less visible during B season mainly due to a weaker surface temperature signal. However, it is during this season (early summer) that the outflow of BSW is maximum but its influence is masked by the strong signal of the eastern Aegean Sea upwelling[2, 10, 19-22].

Additionally, Fig. 5 and Fig. 6 demonstrate the rose diagrams of the in-situ current speed and direction at locations 1 and 2, during all four seasons. These diagrams reveal the highly energetic hydrodynamic status of these sites. The constant changing of the current direction and the variety of measured velocities enforce the fact that the Aegean Sea is an area where multiple scale patterns exist throughout the entire calendar year. These patterns are caused by the combination of the fast time-scale wind effects (mostly present during A seasons) and the slower-scale thermohaline circulation effects (mostly present during B seasons). The distinct impact of these effects during each season is justified by the fact that the

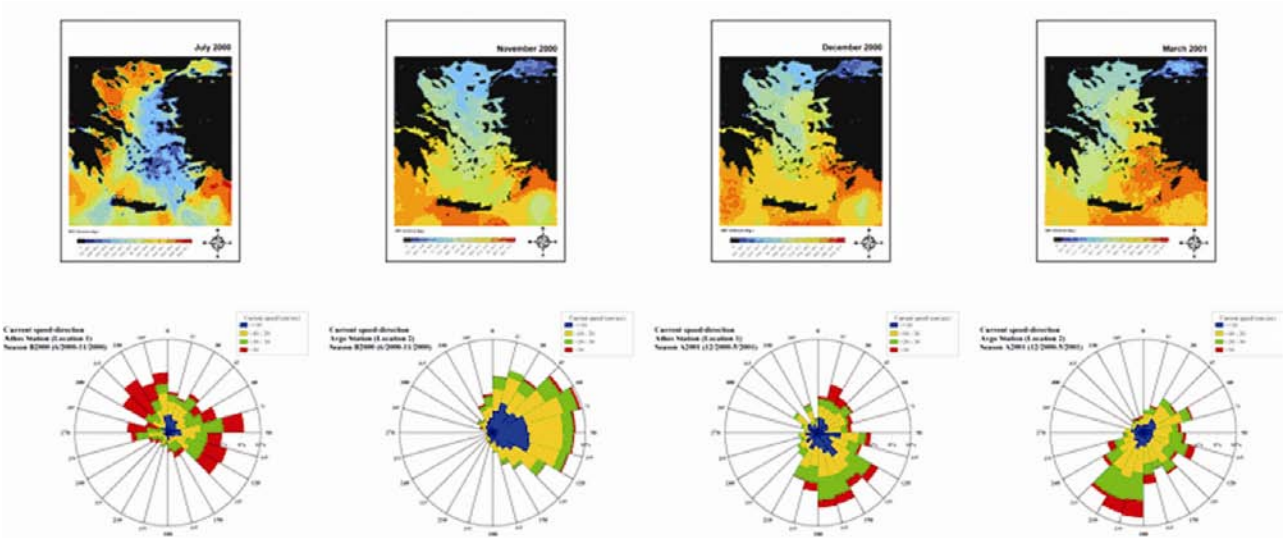

Fig. 5—Representative SST maps of seasons B2000 (first and second column from the left) and A2001 (third and fourth column from the left) and corresponding current rose diagrams for locations 1 and 2

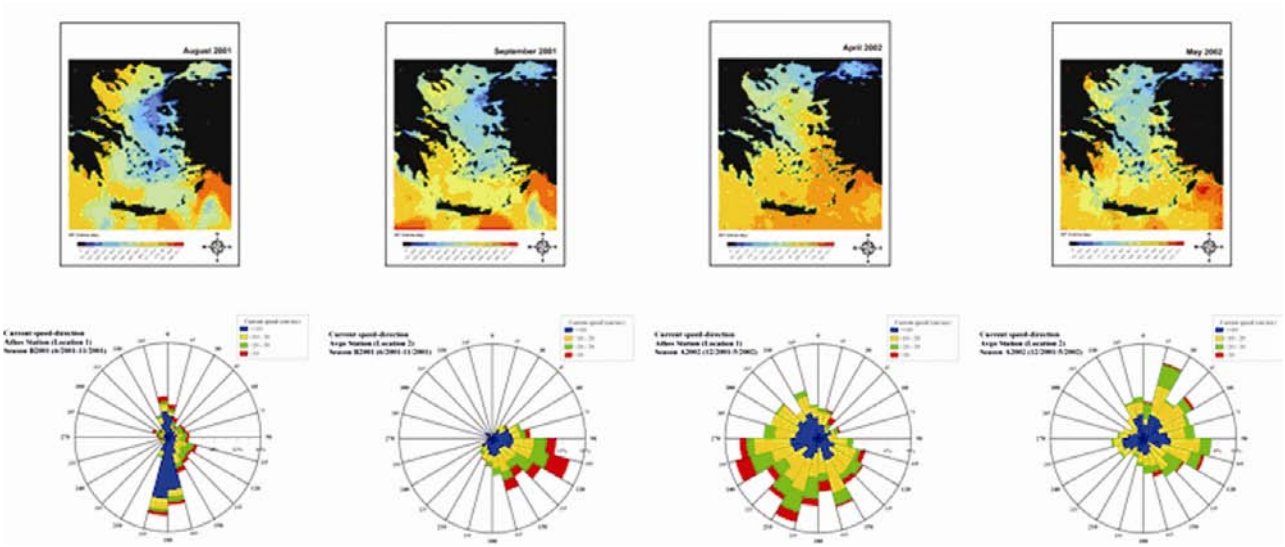

Fig. 6—Representative SST maps of seasons B2001 (first and second column from the left) and A2002 (third and fourth column from the left) and corresponding current rose diagrams for locations 1 and 2

stratification conditions favour buoyancy and thermohaline movements, while mixing conditions favour vertical and horizontal convection as well as turbulent flows.

The combined observation of the rose diagrams with the SST maps shows a fair agreement as far as the general trends of the surface current behaviour are concerned. Moreover, the multiscale circulation trend of the Aegean Sea discussed in former studies (see references in Introduction) is confirmed and the seasonal cycle is testified. For instance, during B seasons at location 2 the existence of the highly active dipole system (warm anticyclone-cold cyclone[23]) is evident. The mooring location coincides with the left (west) part of the cyclonic eddy and so the dominant direction, recorded during the corresponding season, is S-SE.

Directional analysis of surface current and wind in locations 1 and 2

This allows a more detailed study of the fine local surface hydrodynamic conditions. In this respect, directional statistics is the only way of quantifying the relations between sea-surface currents and collocated wind directions. It can be easily applied in any other location where current and wind data are

simultaneously available. The proposed approach when combined with remote sensed SST maps comprises a complete method for the assessment of the surface hydrodynamic conditions in various locations.

In Table 1 the sample size *N*, mean value $\bar{\theta}$, mean length $\bar{R}$, concentration parameter $\hat{k}$, variance *V* and standard deviation *SD* of the surface current direction are presented for each of the examined seasons, namely B2000, A2001, B2001 and A2002, for locations 1 and 2.

As far as the physical meaning of directional statistics of sea surface currents is concerned, it is useful to bear in mind that during stratification B seasons, the meso-scale and large surface structures that meet the general thermohaline circulation are intensified. These structures are almost independent of the prevailing wind conditions and therefore exhibit space and time stability in relation to the constant fluctuations of the wind. On the other hand, during mixing A seasons, the signal of the large and meso-scale patterns is weakened and the small scaled wind driven eddies, mostly dependent on the local wind climate, dominate. These eddies are more unstable, of turbulent nature and continuously changing direction and speed.

Location 1

From Table 1 we see that the characteristics of A and B seasons in location 1 are different, in the mean, for the years 2000 and 2001. The mean current direction for season B changes from 36.995° (for year 2000) to 140.139° (for year 2001). During B2000, the estimated mean current direction, 36.995°, coincides with the coastal movement of warm water masses along the north-west coasts of Greece (Fig. 5 and Fig. 6). The low rated inflow of the BSW during year 2000 intensifies the dominance of the north-east warm current. During B2001 the dominance of the BSW inflow is clearer and thus the estimated mean current direction, 140.139°, coincides with the extensive southerly movement of the cold water masses from the Black Sea (Fig. 5 and Fig. 6).

The mean current direction for season A rotates from 130.572° (for year 2000) to 220.631° (for year 2001). The rather small deviation, most probably results from rationally small deviations of the wind conditions during the mixing seasons of the corresponding years. However, the differences between the mean directions of seasons A and B remain remarkably stable. Stable remain also the standard deviation (slightly fluctuating between 90° and 98°), the concentration parameter $\hat{k}$, as well as the mean length $\bar{R}$, for both seasons and years. The rather low values of the parameters indicate that the distribution of the current direction is widely dispersed for both seasons. Though someone would expect the concentration parameter $\hat{k}$ to be higher for B seasons when large and stable surface patterns dominate, the values in Table 1 indicate the opposite. An explanation for this could be the fact that location 1 is under the influence of the front between the fresh-cold BSW and the warm-saline Aegean Waters. The variability of this front and the transient eddies

Table 1—Directional current statistics in locations 1 and 2 during A, B and aggregated seasons

Statistical parameters		*N*	$\bar{\theta}$	$\bar{R}$	$\hat{k}$	*V*	*SD*
Location	Season						
1	**B2000**	1423	36.995°	0.245	0.506	0.755	96.083°
	A2001	1107	130.572°	0.285	0.595	0.715	90.786°
	B2001	1406	140.139°	0.227	0.466	0.773	98.695°
	A2002	665	220.631°	0.269	0.56	0.731	92.796°
	Aggregated A	1772	160.179°	0.205	0.418	0.795	102.06°
	Aggregated B	2829	85.341°	0.147	0.297	0.853	112.214°
2	**B2000**	1389	71.25°	0.521	1.216	0.479	65.399°
	A2001	1200	160.549°	0.287	0.599	0.713	90.547°
	B2001	719	127.269°	0.553	1.33	0.447	62.391°
	A2002	615	75.372°	0.246	0.508	0.754	95.906°
	Aggregated A	1815	137.624°	0.214	0.437	0.786	100.681°
	Aggregated B	2108	90.452°	0.475	1.078	0.525	69.882°

generated in the area are responsible for the high variability of current fields recorded in location 1. The intensification of this front during the summer period, when the BSW outflow into the Aegean is maximum, can explain the decrease of concentration parameter $\hat{k}$ during B seasons. One more "peculiar" result of Table 1 refers to the values of the concentration parameter $\hat{k}$ for seasons B2000, B2001 and the aggregated season B (2000 and 2001). More precisely, the values of $\hat{k}$ for B2000 and B2001 may be suggesting a dispersed distribution of current direction, but the corresponding value of $\hat{k}$ for the aggregated B season indicates a more dispersed distribution. This seemingly "paradox" most probably results from the significant interannual variability of the BSW front and the resulting differences on the flow regime between periods B2000 and B2001.

Location 2

In location 2 there is a dissimilar situation: the mean current direction for season B rotates from 71.25° (2000) to 127.269° (2001) and for season A from 160.549° to 75.372°, respectively. The difference between the estimated mean current directions depend on the hydrodynamics of the very energetic meso-scale dipole prevailing at the coastal areas north of Crete during B seasons (see Fig. 5 and Fig. 6 and the corresponding comments). On the other hand, the difference that can be traced in the mean current direction for A seasons, depends on the local wind climate dominating during each year.

The standard deviation remains stable for same seasons. The concentration parameter $\hat{k}$ and the mean length $\overline{R}$ are clearly lower during seasons A, indicating that the distribution of the current direction is more clustered around the mean value during the seasons B. This result denotes the dominant presence of the seasonal meso-scale dipole system north of Crete, during stratification seasons; this system is almost stable and independent of wind conditions. The dipole becomes more unstable during the mixing seasons (early A seasons) resulting in reduction of the corresponding concentration parameter $\hat{k}$. During the A seasons, $\hat{k}$, $\overline{R}$, V and SD of both locations are fairly comparable.

From Table 1 it is clear that for location 1 there is an interannual current trend of eastwards rotation. More specifically, the evolution of the estimated mean current directions during the entire period of available data, denote an ongoing clockwise turn, which, from B2000 to A2002, is of the order of 183°. In contrast, for location 2, there is an annual trend which seems to be opposite for years 2000 and 2001. Specifically, from B2000 to A2001 there is a clockwise rotation in the mean current directions of the order of 89°. From B2001 to A2002, though, there is an anticlockwise rotation of the order of 52°. This oscillating "mean" movement could be attributed to the annual variability of the hydrodynamic structure of the Cretan dipole system. It should be noted, however, that the analysis of the two-year dataset is not sufficient enough for deriving safe conclusions on larger time/space scaled movements, trends and phenomena.

Let us now examine the circular-circular correlation structure between wind and current directions and the circular-linear correlations between the speed and directions of the wind and current data. Denote by θ_W the wind direction, θ_C the current direction, u_W the wind speed and u_C the current speed; using Eq. 6 we obtain for location 1 the following results for the circular-circular correlation coefficient:

$r_T(\theta_W, \theta_C | B00) = 0.006$, $r_T(\theta_W, \theta_C | A01) = 0.044$, $r_T(\theta_W, \theta_C | B01) = -0.01$, $r_T(\theta_W, \theta_C | A02) = -0.011$. These results show that the circular-circular correlation coefficient between wind and current directions is extremely low (practically zero) for both seasons. The only conclusion that can be drawn from these results is that the conditions shaping the surface hydrodynamics of the area are triggered from general -wind independent-trends, persisting almost throughout the entire year.

Using Eq. 7 for calculating the circular-linear correlation coefficient we obtain the results summarized in Table 2. From this table the following conclusions can be drawn:

i) The correlation coefficient is higher for wind vectors than for current vectors (wind speed is more correlated with wind direction than current speed with current direction).

ii) The correlation coefficient between wind speed and current direction is, in most cases, by far higher than the correlation coefficient between wind direction and current speed.

iii) The correlation coefficients between current direction and wind/current speed are higher for seasons A than for the corresponding seasons B.

Table 2—Circular-linear correlation coefficient for all seasons for locations 1 and 2
(bold italics indicate estimates obtained from very small sample size)

Direction	Scalar variables / Season							
	LOCATION 1							
	$u_W \mid B00$	$u_C \mid B00$	$u_W \mid A01$	$u_C \mid A01$	$u_W \mid B01$	$u_C \mid B01$	$u_W \mid A02$	$u_C \mid A02$
θ_W	0.437	0.135	0.256	0.066	0.269	0.276	***0.497***	***0.379***
θ_C	0.245	0.165	0.304	0.182	0.212	0.149	***0.504***	***0.483***
	LOCATION 2							
θ_W	0.429	0.108	0.221	0.065	0.364	0.372	0.239	0.268
θ_C	0.236	0.121	0.101	0.254	0.191	0.403	0.128	0.247

Following the same procedure as above for location 2 we obtain the results presented in the last two rows of Table 2. The values $r_T(\theta_W, \theta_C \mid B00) = -0.046$, $r_T(\theta_W, \theta_C \mid A01) = 0.068$, $r_T(\theta_W, \theta_C \mid B01) = 0.309$, $r_T(\theta_W, \theta_C \mid A02) = 0.51$, indicate that the circular-circular correlation coefficients between wind and current directions are higher, in absolute values, than the corresponding ones for location 1. Thus, a more significant interdependence between wind and current direction is revealed in this case. In addition, the higher circular-circular correlation coefficients for seasons A indicate the presence of the wind dependent surface eddies, while the lower correlation coefficients for seasons B indicate the dominance of large and meso-scale, wind independent, patterns. Table 2 infers the following

i) The correlation coefficient is in general (except of season B2000) higher for current vectors than for wind vectors (current speeds are more correlated with current directions than wind speeds with wind directions). This is in contrast with the situation in location 1.
ii) The correlation coefficients of wind speed and wind direction are systematically higher for seasons B than for seasons A.
iii) The correlation coefficients of current speed and direction are almost constant for seasons A, in contrast to seasons B, when they are fairly different. The same remark holds true for wind speed and direction.

Conclusions

The Aegean Sea is a very complex area as far as hydrodynamic conditions are concerned. A lot of numerical results concerning linear parameters, as e.g. wind and current speed, have been presented in previously published works. However, there is a lack in the relevant literature on the numerical assessment of the directional characteristics of these parameters.

In this work the rational combination of in-situ measurements and SST images of the Aegean Sea has been performed and the special features of the surface circulation patterns (seasonality and non-periodicity) are verified and quantified for two specific locations. A directional statistics analysis has been implemented in order to assess numerically the behaviour of the current direction, quantify the specific correlation structures between current and wind directions and reveal the distinguishing seasonal and annual characteristics of the examined areas (during stratification and mixing conditions), always in connection to the general surface circulation. Numerical results showed explicitly that during stratification seasons the surface current directions follow the general, wind-independent and fairly stable, thermohaline trend. During mixing seasons the quite unstable (in both time and space) transient eddies and wind driven currents dominate the circulation of the upper layers of the Aegean Sea. The movement, persistence, duration and signal of the surface circulation patterns has been appeared to be quite different during each season or calendar year, shaping in this way a completely different layout of the overall sea surface circulation. Some interesting aspects concerning the functional structures between the in-situ wind and current speeds and directions lay the foundations for further research and evidently, first-rate knowledge of the hydroynamic laws governing these plonomena is absolutely demanded.

References

1 Johannessen O M, Sandven S, Jenkins A D, Durand D, Pettersson L H, Espedal H, Evensen G & Hamre T, Satellite

earth observation in operational oceanography, *Coast. Eng.*, 41(2000) 155-176.

2 Theocharis A, Georgopoulos D, Lascaratos A & Nittis K, Water masses and circulation in the central region of the Eastern Mediterranean: Eastern Ionian, South Aegean and Northwest Levantine, 1986-1987, *Deep-Sea Res. PT II*, 40(1993) 1121-1142.

3 Schlitzer R, Roether W, Oster H, Junghans H G, Hansmann M & Michelato A, Chlorofluoromethane and oxygen in the Eastern Mediterranea, *Deep-Sea Res.*, 38 (1991) 1531-1551.

4 Roether W, Manca B, Klein B, Bregant D, Georgopoulos D, Beitzel V, Kovacevic V & Luchetta A, Recent changes in the Eastern Mediterranean deep waters, *Science*, 271 (1996) 333-335.

5 Theocharis A, Balopoulos E, Kioroglou S, Kontoyiannis H & Iona A, A synthesis of the circulation and hydrology of the South Aegean Sea and the Straits of the Cretan Arc (March 1994-January 1995), *Prog. Oceanogr.*, 44 (1999) 469-509.

6 Lascaratos A, Sofianos S & Korres G, Interannual variability of atmospheric parameters over the Mediterranean basin from 1945 to 1994, in *Tracking long-term hydrological change in the Mediterranean Sea*, edited by Briand, F, (CIESM Workshop Series, Monaco), 16 (2002) pp. 21-24.

7 Malanotte-Rizzoli P, Manca B, Ribera d' Alcala M, Theocharis A, Bergamasco A, Bregant D, Budillon G, Civitanese G, Georgopoulos D, Michelato A, Sansone E, Scarazzato P & Souvermezoglou E, A synthesis of the Ionian Sea hydrography, circulation and water mass pathways during POEM-Phase I, *Prog. Oceanogr.*, 39 (1997) 153-204.

8 Zervakis V, Georgopoulos D & Drakopoulos P G, The role of the North Aegean Sea in triggering the recent Eastern Mediterranean climatic changes, *J. Geophys. Res.*, 105 (2000) 26103-26116.

9 Georgopoulos D, Zervakis V, Theocharis A, Nittis K, Perivoliotis L & Papadopoulos A, The monitoring of the evolution of the hydrological characteristics in the deep basins of the North Aegean Sea, in *Tracking long-term hydrological change in the Mediterranean Sea*, edited by Briand, F, (CIESM Workshop Series, Monaco), 16 (2002), pp. 79-81.

10 Nittis K & Perivoliotis L, Circulation and hydrological characteristics of the North Aegean Sea: a contribution from real-time buoy measurements, *Mediterranean Marine Science*, 3 (2002) 21-31.

11 Kourafalou V H & Barbopoulos K, High resolution simulations on the North Aegean Sea seasonal circulation, *Ann. Geophys.*, 21(2003) 251-265.

12 Soukissian T, Chronis G & Nittis K, POSEIDON: Operational marine monitoring system for the Greek seas, *Sea Technology*, 40 (1999) 31-37.

13 Mcclain E P, Pichel W G & Walton C C, Comparative performance of AVHRR-based multichannel sea surface temperatures, *J. Geophys. Res.*, 80(1985) 5113-5117.

14 Mardia K V, *Statistics of directional data*, (Academic Press, London) 1972, pp. 360.

15 Fisher N I & Lee A J, A correlation coefficient for circular data, *Biometrica*, 70(1983) 327-332.

16 Fisher N I, *Statistical analysis of circular data*, (Cambridge University Press, New York) 1995, pp 296.

17 Mardia K V & Jupp P, *Directional Statistics*, (John Wiley and Sons, 2nd edition, New York) 2000, pp. 350.

18 Nittis K, Pinardi N & Lascaratos A, Characteristics of the summer 1987 flow field in the Ionian Sea, *J. Geophys. Res.*, 98(1993) 171-184.

19 Hopkins T S, Physical processes in the Mediterranean basins, in *Estuarine transport processes*, edited by B. Kjerfve, (University of South Carolina Press), 1978, pp. 269-310.

20 Georgopoulos D, Salusti E & Theocharis A, Dense water formation processes in the North Aegean Sea (Eastern Mediterranean), *Ocean Model.*, 95(1992) 4-6.

21 Zodiatis G & Balopoulos E, Structure and characteristics of fronts in the North Aegean Sea, *Bolletino in Oceanologica Theorica ed Applicata*, XI(1993) 113-124.

22 Zodiatis G, Advection of the Black Sea water in the North Aegean Sea, *Global Atmos, Ocean Syst.*, 2(1994) 41-60.

23 Cardin V, Gacic M, Nittis K, Kovacevic V & Perini L, Sub-inertial variability in the Cretan Sea from M3A buoy, *Ann. Geophys.*, 21(2002) 89-102.